





Structured liquids stabilized by polyethyleneimine surfactants†

Cite this: *Soft Matter*, 2023, 19, 609

Received 29th November 2022,
Accepted 7th January 2023

DOI: 10.1039/d2sm01559e

rsc.li/soft-matter-journal

Mingwei Li,^a Shuyi Sun,^a Rongrong Qin,^c Meng Wang,^c Yongkang Wang,^b
Yang Yang,^a Zhanpeng Wu ^{*b} and Shaowei Shi ^{*ad}

Using host–guest interactions between β -cyclodextrin-modified branched polyethyleneimine and ferrocene-terminated poly-L-lactide, the formation, assembly and jamming of polyethyleneimine surfactants (PEISs) at the liquid–liquid interface is presented. With PEIS, reconfigurable liquids with electrochemical redox responsiveness can be constructed. In conjunction with microfluidic methods, continuous, selective diffusion and purification of ionic species can be achieved in all-liquid constructs.

Liquids, by definition, display the properties of fluids and adopt the shape of their containers. Shaping liquids into prescribed architectures and reconfiguring them on-demand would enable the design of a new class of soft materials, where the desirable characteristics of fluids are combined with the structural stability of a solid.¹ A promising route to this goal is the use of nanoparticle surfactants (NPSs) in liquid–liquid systems.² NPSs are formed when nanoparticles and polymer/oligomer ligands, each dispersed into separate immiscible liquids and having complementary functionality, interact with one another at the liquid–liquid interface. Here, NPSs act as standard surfactants by decreasing the interfacial tension and, due to the self-regulated number of ligands anchored to the nanoparticles, the binding energy of NPSs is significantly enhanced. When decreasing the interfacial area to compress the assembly of NPSs, the NPSs are not ejected from the interface but jam, transforming the interfacial assemblies from “liquid-like” to “solid-like”, allowing the stabilization of liquids

in highly non-equilibrium shapes, that is, structured liquids.³ By using different types of interactions between nanoparticles and ligands, such as electrostatic interactions and host–guest interactions, structured liquids can be responsive to various external stimuli, such as ionic strength, pH, photo, and redox, leading to a switchable jamming-to-unjamming transition of NPSs and enabling a further reshaping of the liquids.⁴

As the formation of NPSs is independent of the chemical nature or shape of nanoparticles, a variety of inorganic (*e.g.*, SiO₂, Au, Fe₃O₄, MXene) and organic nanoparticles (polystyrene, cellulose nanocrystals) have been used to generate NPSs, then to construct structured liquids, where the inherent properties of nanoparticles are integrated into the resultant assemblies.⁵ In comparison to nanoparticles, functional polymers would be more efficient building blocks, due to the advantages of low cost, structural diversity and facile chemical modification.⁶ Recently, by using the electrostatic interactions between a negatively charged polyelectrolyte (*e.g.*, DNA, sodium carboxymethyl cellulose) and a positively charged ligand to form polyelectrolyte surfactants (PESs), emulsions and structured liquids have been prepared.⁷ However, to ensure the interfacial activity of PESs as well as the structural integrity of assemblies, a low pH value of the aqueous phase is usually required, restricting the applications for encapsulating or immobilizing pH-sensitive materials. On the other hand, due to the viscoelastic nature of polymers, by interfacial compression, the jammed assembly of PESs can be gradually relaxed by a reorganization of the PESs, leading to a shape evolution of liquids from nonequilibrium to equilibrium. To address such issues, introducing other types of interactions to form PESs as well as increasing the rigidity of polymer chains would be preferred.

To this end, water-soluble β -cyclodextrin (β -CD)-modified branched polyethyleneimine (PEI- β -CD) and oil-soluble ferrocene (Fc)-terminated poly-L-lactide (Fc-PLLA) were prepared to form a new type of PES, termed PEI surfactant (PEIS), at the oil–water interface (Fig. 1). The host–guest interactions between β -CD and Fc not only trigger the formation and assembly of PEIS, but also endow the resultant interfacial assemblies with redox

^a Beijing Advanced Innovation Center for Soft Matter Science and Engineering, Beijing University of Chemical Technology, Beijing 100029, China. E-mail: shisw@mail.buct.edu.cn

^b State Key Laboratory of Organic–Inorganic Composites, Beijing University of Chemical Technology, Beijing 100029, China. E-mail: wuzp@mail.buct.edu.cn

^c Beijing Xinfeng Aerospace Equipment Co., Ltd, Beijing, 100854, China

^d Beijing Engineering Research Center for the Synthesis and Applications of Waterborne Polymers, Beijing University of Chemical Technology, Beijing 100029, China

† Electronic supplementary information (ESI) available. See DOI: <https://doi.org/10.1039/d2sm01559e>

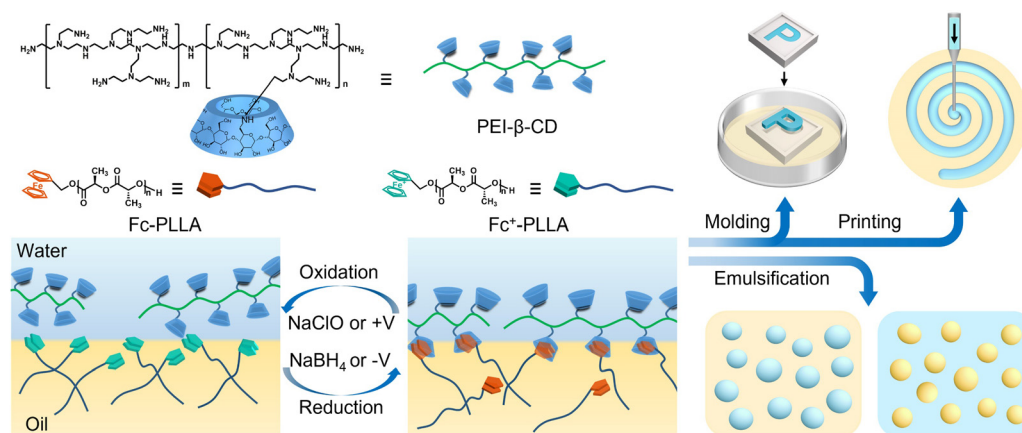


Fig. 1 Schematic representation of the assembly/disassembly of PEIS at the oil–water interface in a redox process, and the preparation of liquid letter, liquid spiral and different types of emulsions.

responsiveness. By applying alternative stimuli of a positive potential (or an oxidant) and a negative potential (or a reductant), switchable emulsification and demulsification can be easily achieved, showing a promising application for encapsulation and release. Due to the rigidity of β-CD, the relaxation of PEIS jammed at the interface can be significantly suppressed, enabling the precise fabrication of structured liquids, by either 3D printing⁸ or molding method.⁹ Moreover, by taking advantage of the high adsorption capacity of PEIS for anionic substances, the separation or purification in prepared all-aqueous systems can be realized in a very simple, efficient manner.

Detailed synthetic procedures of PEI-β-CD and Fc-PLLA are provided in ESI† (Scheme S1 and Fig. S1–S6). The kinetics of PEIS formation and assembly at the toluene–water interface was measured by tracking the dynamic interfacial tension using

pendant drop tensiometry. As shown in Fig. 2a and b, with PEI-β-CD dissolved in water (pH ~ 8.5) against pure toluene, the interfacial tension (33 mN m^{-1}) is close to that of the pure water–toluene system (35 mN m^{-1}), indicating the weak interfacial activity of PEI-β-CD. On the other hand, Fc-PLLA acts as a surfactant due to the formation of hydrogen bonding between PLLA carbonyl groups and water, spontaneously assembling at the toluene–water interface and reducing the interfacial tension to 24 mN m^{-1} . With PEI-β-CD dissolved in water and Fc-PLLA dissolved in toluene, respectively, the interfacial tension reduces further (11 mN m^{-1}), indicating the triggering of the host–guest interactions between β-CD and Fc, and the formation of PEIS at the toluene–water interface. With PEIS assembling at the interface for 600 s, when the volume of the pendant droplet is reduced to compress the interfacial assembly, wrinkles are observed on the

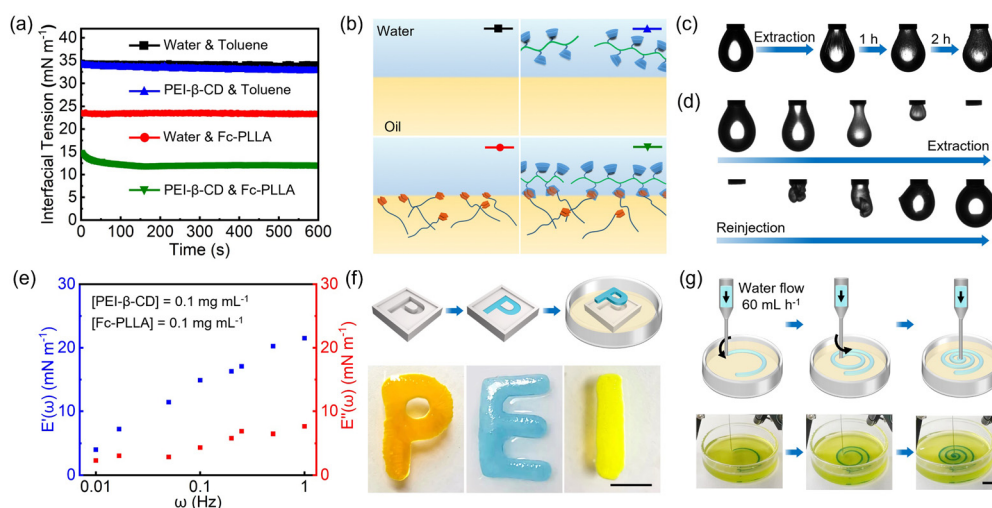


Fig. 2 (a) Time evolution of interfacial tension of different oil–water systems including water/toluene, PEI-β-CD@water/toluene, water/Fc-PLLA@toluene and PEI-β-CD@water/Fc-PLLA@toluene. (b) Schematics of different oil–water systems in (a). (c) Morphology evolution of the pendant droplet with wrinkles on the surface. (d) A series of snapshots showing the shape evolution of a pendant droplet in an extraction–reinjection process; [PEI-β-CD] = 0.1 mg mL^{-1} , [Fc-PLLA] = 1.0 mg mL^{-1} . (e) Storage and loss dilatational moduli, $E'(\omega)$ and $E''(\omega)$ of PEIS-based interfacial assemblies, [PEI-β-CD] = 0.1 mg mL^{-1} , [Fc-PLLA] = 0.1 mg mL^{-1} , $\omega = 0.01\text{--}1 \text{ Hz}$. (f) Schematic diagram and optical images of liquid letters “PEI” fabricated by all-liquid molding, [PEI-β-CD] = 5.0 mg mL^{-1} , [Fc-PLLA] = 5.0 mg mL^{-1} . (g) Schematic diagram and optical images of the prepared liquid spiral, [PEI-β-CD] = 20 mg mL^{-1} , [Fc-PLLA] = 20 mg mL^{-1} . Scale bar: 1.0 cm .

droplet surface immediately and do not relax for over two hours, indicating the surface coverage of PEIS is nearly 100% and, when PEIS jams at the interface, the reorganization of PEIS is significantly inhibited (Fig. 2c). By varying the concentration of either PEI or Fc-PLLA, the kinetics of PEIS formation and assembly can be well adjusted (Fig. S7, ESI†).

The mechanical strength of the PEIS-based interfacial assemblies is investigated by an extraction–reinjection experiment, where the aqueous solution in the pendant droplet is extracted first, then reinjected to generate a new pendant droplet. As shown in Fig. 2d, a large deformation of the interface is observed, demonstrating the robust nature of the interfacial assemblies, which can be used to shape liquids. To quantify the mechanical properties of the interfacial assemblies, the storage moduli $E'(\omega)$ and loss moduli $E''(\omega)$ were measured by oscillatory pendant drop tensiometry/rheometry at low concentrations of PEI- β -CD and Fc-PLLA. Fig. 2e shows that, in the frequency range of 0.01 to 1 Hz, both viscous ($E''(\omega)$) and elastic ($E'(\omega)$) components are obtained, with elastic part being the dominant component, demonstrating the elastic nature of the interfacial assemblies. By taking advantage of the jamming of PEIS at the interface, macroscopic structured liquids including liquid letters “PEI” and liquid spiral can be successfully constructed

by all-liquid molding or 3D printing, with excellent structural stability (Fig. 2f and g).

Emulsions were prepared by vigorously homogenizing the aqueous solution containing PEI- β -CD and toluene solution containing Fc-PLLA. No stable emulsions can be obtained when using only PEI- β -CD or Fc-PLLA. At a constant volume ratio of water and toluene, by varying the mass ratio of PEI- β -CD to Fc-PLLA from 1/10 to 10/1, the hydrophilic–lipophilic balance of PEIS at the interface can be effectively adjusted, leading to the evolution of the emulsion from water-in-oil (W/O) to oil-in-water (O/W), as evidenced by the fluorescent signals of fluorescein sodium dissolved in the aqueous phase and Nile red dissolved in toluene solution (Fig. 3). By fixing the concentrations of PEI- β -CD (1.0 mg mL^{-1}) and Fc-PLLA (1.0 mg mL^{-1}) and varying the volume ratio of water to toluene from 1/10 to 10/1, W/O and O/W emulsions can also be obtained (Fig. 4). We note that, under certain conditions, the shape of emulsion droplet is not spherical, *i.e.*, structured emulsions, which is due to the interfacial jamming of the PEIS during the solution shearing.^{5d} All the emulsions studied have good stability and the non-equilibrium shapes are retained for more than 7 days (Fig. S8–S10, ESI†).

Since β -CD can strongly bind with uncharged Fc (reduced state) through host–guest interactions, but only weakly interacts

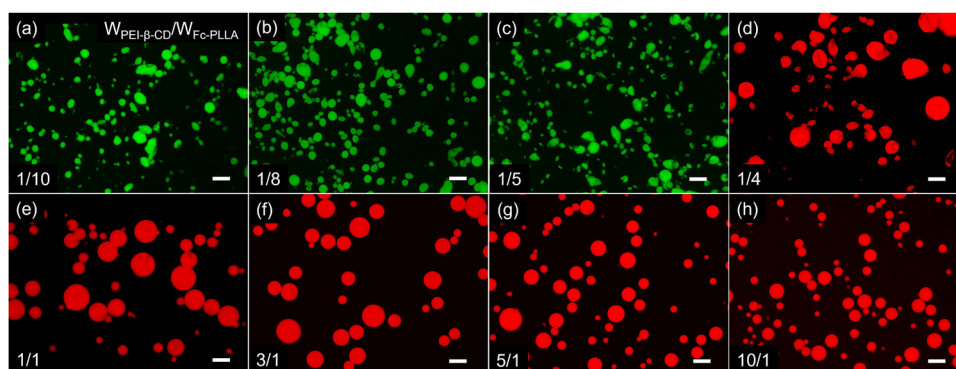


Fig. 3 (a–h) Fluorescence microscopy images of different types of emulsions with different mass ratio of PEI- β -CD to Fc-PLLA from 1/10 to 10/1 at a constant 1/1 volume ratio of water and toluene, where Fluorescein sodium is loaded in water and Nile red is loaded in toluene. [Fluorescein sodium] = 0.5 mg mL^{-1} , [Nile red] = 0.5 mg mL^{-1} , Shear rate = 15 000 rpm, shear time = 2.0 min, scale bar: 100 μm .

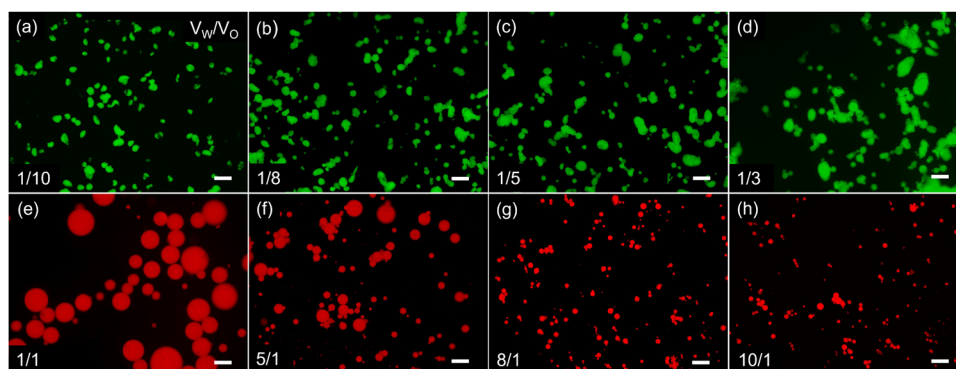


Fig. 4 (a–h) Fluorescence microscopy images of different types of emulsions at different water–oil volume ratios, where Fluorescein sodium is loaded in water and Nile red is loaded in toluene. [PEI- β -CD] = 1.0 mg mL^{-1} , [Fc-PLLA] = 1.0 mg mL^{-1} , [Nile red] = 0.5 mg mL^{-1} , [Fluorescein sodium] = 0.5 mg mL^{-1} , shear rate = 15 000 rpm, shear time = 2.0 min, scale bar: 100 μm .

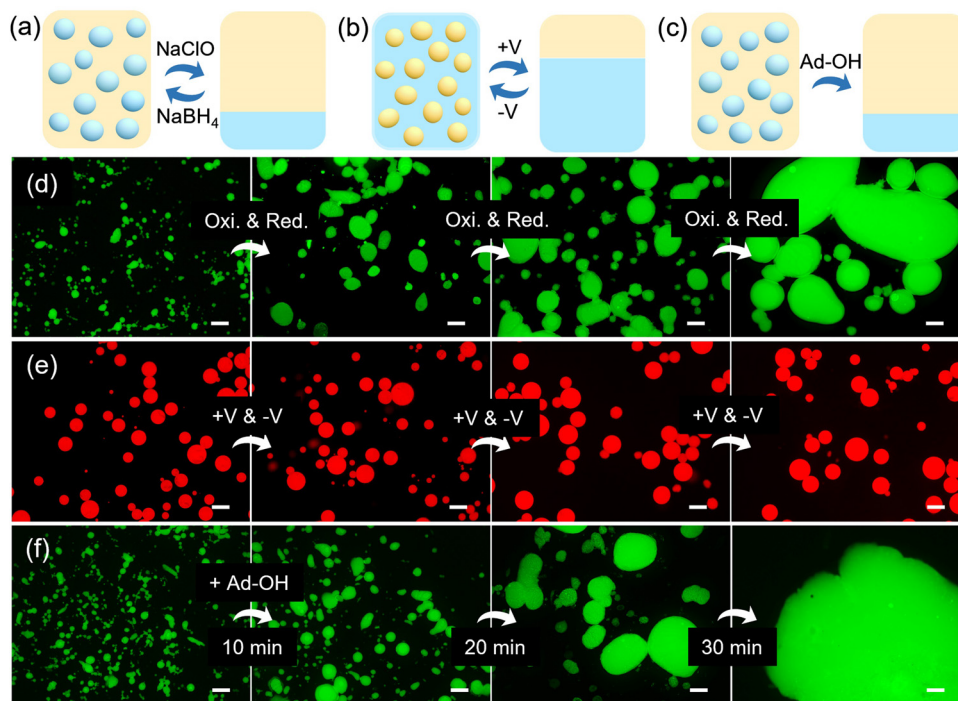


Fig. 5 (a–c) Schematic diagram of switchable demulsification/emulsification process triggered by redox reagent, voltage and competitive guests. (d) Fluorescence microscopy images of emulsions during three redox cycles by the addition of redox reagents, $V_W/V_O = 1:6$, $[\text{NaClO}] = 2.0 \text{ mg mL}^{-1}$, $[\text{NaBH}_4] = 4.0 \text{ mg mL}^{-1}$. (e) Fluorescence microscopy images of emulsions during three redox cycles by applying voltage, $V_W/V_O = 2:1$. (f) The evolution of emulsions droplets morphology after the addition of Ad-OH, $V_W/V_O = 1:6$, $[\text{Ad-OH}] = 2.0 \text{ mg mL}^{-1}$, $[\text{PEI-}\beta\text{-CD}] = 1.0 \text{ mg mL}^{-1}$, $[\text{Fc-PLLA}] = 1.0 \text{ mg mL}^{-1}$. Scale bar: $200 \mu\text{m}$.

with the charged Fc^+ (oxidized state). The association and dissociation of PEIS at the interface can be reversibly manipulated by a redox process, endowing the interfacial assemblies with redox responsiveness.¹⁰ As shown in Fig. 5a, d and Fig. S11 (ESI[†]), with the repeated addition of the oxidant, sodium hypochlorite (NaClO), and the reductant, sodium borohydride (NaBH_4), to the W/O emulsions stabilized by PEIS, a switchable demulsification/emulsification can be achieved. However, it is observed that, as the number of cycles increases, the size of emulsion droplets increases slightly in comparison to that of original emulsions, which is due to the insufficient reduction of Fc^+ -PLLA and less formation of PEIS at the interface. In comparison to the redox reagents, an electrochemical redox trigger has been considered as a “green” method, making it favorable to be used in biological systems. The electrochemical controlled demulsification/emulsification experiments are performed by inserting three electrodes into the O/W emulsions and using voltage as the stimuli.¹¹ As shown in Fig. 5b and e and Fig. S12 (ESI[†]), when repeatedly applying a positive voltage and a negative voltage to the emulsions, a switchable demulsification/emulsification is also obtained but the size of emulsion droplets remains unchanged with the increasing number of cycles, demonstrating the advantages of an electrochemical stimulus. On the other hand, guest-competitive responsiveness can be achieved by adding a competitive guest, adamantane methanol (Ad-OH), to the W/O emulsions, due to the higher association constant of adamantane for $\beta\text{-CD}$ than that of Fc for $\beta\text{-CD}$.¹²

As shown in Fig. 5c and f, with the addition of Ad-OH, the emulsion droplets coalesce immediately, indicating the binding energy of newly formed PEI- $\beta\text{-CD}$ /Ad-OH complex is insufficient to stabilize the interface.

By taking advantage of the high adsorption capacity of PEI (positively charged) for anionic substances, the separation or purification of ionic species was investigated in a 3D printed all-liquid microfluidic chip.^{8d,13} A mixed aqueous solution of Rose Bengal (RB, negatively charged) and Methylene blue (MB, positively charged) was injected through the inlet of the channel and then extracted from the outlet, at a fixed flow rate (3.0 mL h^{-1}) to keep the fluid volume in the channel constant (Fig. 6a–c). In comparison to the purple solution infused from the channel inlet, an obvious color change from purple to blue was observed for the solution collected from the channel outlet, indicating the negatively charged RB has been adsorbed onto the inner wall of channel and only positively charged MB is collected. This result can be supported by the UV-vis absorption spectra of the infused and collected solutions. As shown in Fig. 6d and Fig. S13 (ESI[†]), for the solution collected from the outlet, the absorption peak of RB almost disappears, while that of MB remains. The separation of ionic species can also be achieved by adding the mixed solution of RB and MB to O/W emulsions (Fig. 6e). After stirring the emulsions for a while, it is found that RB is mainly adsorbed onto the surface of creamed emulsion droplets (the upper layer), and MB remains in the continuous phase (the bottom layer). The adsorption efficiency

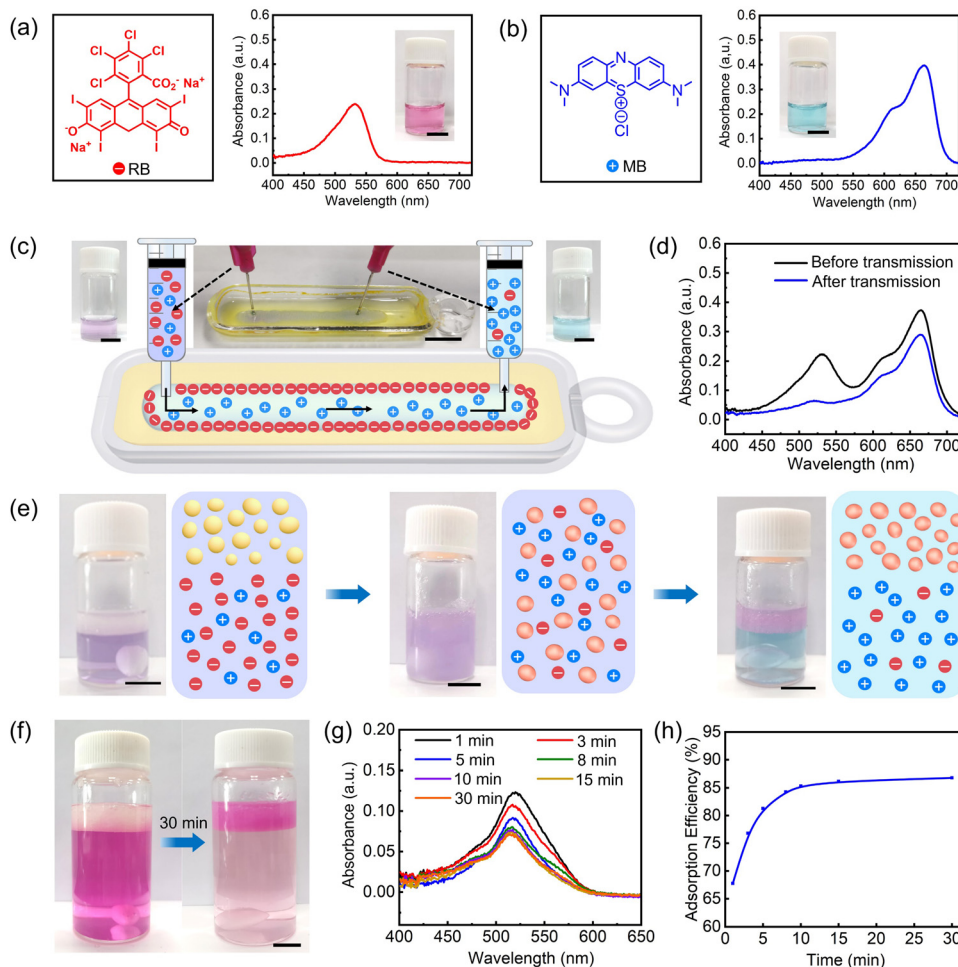


Fig. 6 Chemical structures and UV-vis absorption spectra of (a) RB and (b) MB. (c) Schematic diagram and optical image of 3D printed all-liquid microfluidic chip for separation of ionic species, flow rate = 3.0 mL h⁻¹. (d) UV-vis absorption spectra of RB/MB-containing aqueous solutions before and after transmission. (e) Schematic diagrams and optical images of emulsions for the separation of ionic species. (f) Optical images showing the adsorption of RB by emulsions. (g and h) Adsorption spectra of RB-containing aqueous solutions and adsorption efficiency of RB with time, [PEI-β-CD] = 1.0 mg mL⁻¹, [Fc-PLLA] = 1.0 mg mL⁻¹, V_W/V_O = 2 : 1, [RB] = 0.025 mg mL⁻¹, [MB] = 0.0084 mg mL⁻¹, scale bar: 1.0 cm.

of the O/W emulsions is investigated by measuring the absorption intensity of RB at different times. As shown in Fig. 6f–h, by adding an RB-containing aqueous solution to the O/W emulsions, the absorption intensity of RB reduced with time and ~85% RB had been adsorbed in 30 min.

In summary, by taking advantage of the host-guest interactions between PEI-β-CD and Fc-PLLA, we report the *in situ* formation, assembly and jamming of PEIS at the toluene–water interface. Due to the rigid nature of PEIS, when jammed, the relaxation of PEIS-based interfacial assemblies can be effectively suppressed, enabling the construction of structured liquids. The assembly/jamming and disassembly/unjamming of PEIS can be reversibly controlled by applying voltage or using redox reagent, endowing the prepared emulsions with dual redox responsiveness. Moreover, by taking advantage of the high adsorption capacity of PEIS for anionic substances, the selective separation and purification of ionic species can be realized using the 3D-printed all-liquid microfluidic chip or emulsions. In comparison to conventional NPSs or PES, PEIS providing a more efficient and rigid platform

for construction of programmable liquids with potential applications in encapsulation, cargo release, and chemical separations.

Conflicts of interest

There are no conflicts to declare.

Acknowledgements

This work was supported by the Beijing Natural Science Foundation (2222071) and the National Natural Science Foundation of China (52173018, 51903011). We are grateful to Prof. Thomas P. Russell at University of Massachusetts Amherst for insightful discussions.

Notes and references

- 1 P. G. de Gennes, *Science*, 1992, **256**, 495–497.

- 2 M. M. Cui, T. Emrick and T. P. Russell, *Science*, 2013, **342**(6157), 460–463.
- 3 (a) S. W. Shi and T. P. Russell, *Adv. Mater.*, 2018, **30**, 1800714; (b) S. Y. Sun, T. Liu, S. W. Shi and T. P. Russell, *Colloid Polym. Sci.*, 2021, **299**, 523–536; (c) J. Forth, P. Y. Kim, G. H. Xie, X. B. Liu, B. A. Helms and T. P. Russell, *Adv. Mater.*, 2019, **31**, e1806370.
- 4 (a) Y. Chai, A. Lukito, Y. F. Jiang, P. D. Ashby and T. P. Russell, *Nano Lett.*, 2017, **17**, 6453–6457; (b) C. L. Huang, Z. W. Sun, M. M. Cui, F. Liu, B. A. Helms and T. P. Russell, *Adv. Mater.*, 2016, **28**, 6612–6618; (c) H. L. Sun, L. S. Li, T. P. Russell and S. W. Shi, *J. Am. Chem. Soc.*, 2020, **142**, 8591–8595; (d) H. L. Sun, M. W. Li, L. S. Li, T. Liu, Y. Z. Luo, T. P. Russell and S. W. Shi, *J. Am. Chem. Soc.*, 2021, **143**(10), 3719–3722; (e) Y. Z. Luo, Y. Yang, Y. K. Wang, Z. P. Wu, T. P. Russell and S. W. Shi, *Angew. Chem., Int. Ed.*, 2022, **61**, e202207199.
- 5 (a) X. B. Liu, N. Kent, A. Ceballos, R. Streubel, Y. F. Jiang, Y. Chai, P. Y. Kim, J. Forth, F. Hellman, S. W. Shi, D. Wang, B. A. Helms, P. D. Ashby, P. Fischer and T. P. Russell, *Science*, 2019, **365**, 264–267; (b) S. W. Shi, B. Q. Qian, X. Y. Wu, H. L. Sun, H. Q. Wang, H. B. Zhang, Z. Z. Yu and T. P. Russell, *Angew. Chem., Int. Ed.*, 2019, **58**, 18171; (c) C. L. Huang, M. M. Cui, Z. W. Sun, F. Liu, B. A. Helms and T. P. Russell, *Langmuir*, 2017, **33**, 7994–8001; (d) Y. N. Li, X. B. Liu, Z. Zhang, S. J. Zhao, G. F. Tian, J. K. Zheng, D. Wang, S. W. Shi and T. P. Russell, *Angew. Chem., Int. Ed.*, 2018, **57**, 13560.
- 6 M. Q. Hu and T. P. Russell, *Mater. Chem. Front.*, 2021, **5**, 1205–1220.
- 7 (a) B. Q. Qian, S. W. Shi, H. Q. Wang and T. P. Russell, *ACS Appl. Mater. Interfaces*, 2020, **12**(11), 13551–13557; (b) R. Y. Xu, T. Liu, H. L. Sun, B. B. Wang, S. W. Shi and T. P. Russell, *ACS Appl. Mater. Interfaces*, 2020, **12**(15), 18116–18122.
- 8 (a) X. B. Liu, S. W. Shi, Y. N. Li, J. Forth, D. Wang and T. P. Russell, *Angew. Chem., Int. Ed.*, 2017, **56**, 12594; (b) J. Forth, X. B. Liu, J. Hasnain, A. Toor, K. Miszta, S. W. Shi, P. L. Geissler, T. Emrick, B. A. Helms and T. P. Russell, *Adv. Mater.*, 2018, **30**, 1707603; (c) W. Q. Feng, Y. Chai, J. Forth, P. D. Ashby, T. P. Russell and B. A. Helms, *Nat. Commun.*, 2019, **10**, 1905; (d) T. Liu, Y. X. Yin, Y. Yang, T. P. Russell and S. W. Shi, *Adv. Mater.*, 2022, **34**, 2105386.
- 9 S. W. Shi, X. B. Liu, Y. N. Li, X. F. Wu, D. Wang, J. Forth and T. P. Russell, *Adv. Mater.*, 2018, **30**, 1705800.
- 10 M. Nakahata, Y. Takashima, H. Yamaguchi and A. Harada, *Nat. Commun.*, 2011, **2**, 511.
- 11 (a) T. Matsue, D. H. Evans, T. Osa and N. Kobayashi, *J. Am. Chem. Soc.*, 1985, **107**(12), 3411–3417; (b) A. Harada, *Acc. Chem. Res.*, 2001, **34**(6), 456–464; (c) Q. Yan, J. Y. Yuan, Z. N. Cai, Y. Xin, Y. Kang and Y. W. Yin, *J. Am. Chem. Soc.*, 2010, **132**(27), 9268–9270; (d) L. Peng, A. C. Feng, S. Y. Liu, M. Huo, T. Fang, K. Wang, Y. Wei, X. S. Wang and J. Y. Yuan, *ACS Appl. Mater. Interfaces*, 2016, **8**(43), 29203–29207.
- 12 (a) M. V. Rekharsky and Y. Inoue, *Chem. Rev.*, 1998, **98**, 1875–1918; (b) J. S. Wu, K. Toda, A. Tanaka and I. Sanemasa, *Bull. Chem. Soc.*, 1998, **71**, 1615–1618; (c) B. B. Wang, B. Q. Yin, Z. Zhang, Y. X. Yin, Y. Yang, H. Q. Wang, T. P. Russell and S. W. Shi, *Angew. Chem., Int. Ed.*, 2022, **61**, e202114936.
- 13 (a) R. Krishnamoorthi, R. Anbazhagan, H. C. Tsai, C. F. Wang and J. Y. Lai, *J. Taiwan. Inst. Chem. Eng.*, 2021, **118**, 325–333; (b) Z. G. Zhu, P. Wu, G. J. Liu, X. F. He, B. Y. Qi, G. F. Zeng, W. Wang, Y. H. Sun and F. Y. Cui, *Chem. Eng. J.*, 2017, **313**, 957–966; (c) W. Wang, Q. Bai, T. Liang, H. Y. Bai and X. Y. Liu, *Polymers*, 2017, **9**(9), 455; (d) S. Wong, H. H. Tumari, N. Ngadi, N. B. Mohamed, O. Hassan, R. Mat and N. A. S. Amin, *J. Cleaner Prod.*, 2019, **206**, 394–406.